Physica D 260 (2013) 112–126

Contents lists available at ScienceDirect

Physica D

journal homepage: www.elsevier.com/locate/physd

A new interaction potential for swarming models

J.A. Carrillo [a], S. Martin [a,*], V. Panferov [b]

[a] Department of Mathematics, Imperial College London, London SW7 2AZ, UK

[b] Department of Mathematics, California State University Northridge, Northridge, CA 91330-8313, USA

ARTICLE INFO

Article history:
Available online 18 February 2013

Keywords:
Swarming patterns
Individual based models
Self-propelled interacting particles
Quasi-Morse potentials

ABSTRACT

We consider a self-propelled particle system which has been used to describe certain types of collective motion of animals, such as fish schools and bird flocks. Interactions between particles are specified by means of a pairwise potential, repulsive at short ranges and attractive at longer ranges. The exponentially decaying Morse potential is a typical choice, and is known to reproduce certain types of collective motion observed in nature, particularly aligned flocks and rotating mills. We introduce a class of interaction potentials, that we call Quasi-Morse, for which flock and rotating mills states are also observed numerically, however in that case the corresponding macroscopic equations allow for explicit solutions in terms of special functions, with coefficients that can be obtained numerically without solving the particle evolution. We compare the obtained solutions with long-time dynamics of the particle systems and find a close agreement for several types of flock and mill solutions.

1. Introduction

Emerging behaviors in interacting particle systems have received a lot of attention in research in recent years. Topics range from diverse fields of applications such as animal collective behavior, traffic, crowd dynamics and crystallization. Self-organization in the absence of leaders has been reported in several species which coordinate their movement (swarming), and several models have been proposed for their explanation [1–6].

Many of these models are based on zones in which some of 3 basic effects are included: short-range repulsion, long-range attraction, and alignment. These 3-zone basic descriptions have been very popular for modeling fish schools [7–11], starlings [12], or ducks [13,14]. The main modeling issues are if some or all of these effects between agents have to be included and if so, how to incorporate them. Many basic swarming models rely on averaged spatial distance or orientation interactions while recent biological studies point out the importance of nearest-neighbor interactions [15] or anisotropic communication [16]. Mathematicians have started in recent years to attack one of the most striking features of these *simple looking* models: the diversity of swarming states, also called patterns in the biology community, their emergence and stability.

The individual level description of these phenomena leads to certain particle systems, called Individual Based Models (IBMs), with some common aspects. Typically, the attraction–repulsion is modeled through pairwise effective potentials depending on the distance between individuals. An asymptotic speed for particles is imposed either by working in the constrained set of a sphere in velocity space [17–19] or by adding a term of balance between self-propulsion and friction which effectively fixes the speed to a limiting value for large times [20,21]. In this work, we will not include any alignment mechanism. We refer to [22] for a survey on results related to kinetic modeling in swarming.

In Section 2 we will review some of these IBMs, and discuss the appearance of two main swarming patterns: mills and flocks. These patterns are easily observed in particle simulations [21,23] and reported in detail for certain particular potentials, the so-called Morse potentials. We will give a precise definition of flocks and mills as solutions of the kinetic equation associated to the particle systems. Finding the spatial shape of flocks and mills has been numerically reported in the literature, but obtaining analytical results on them has only been done in one dimension for the Morse potential in [24].

In this work, we generalize the strategy in [24] proposing a new interaction potential, that we call Quasi-Morse, to replace the Morse potential. The Quasi-Morse potential coincides with the Morse potential in one dimension and we will show that, it is a suitable extension

* Corresponding author. Tel.: +44 0 20 759 48396; fax: +44 0 20 759 48517.
E-mail addresses: carrillo@imperial.ac.uk (J.A. Carrillo), stephan.martin@imperial.ac.uk (S. Martin), vladislav.panferov@csun.edu (V. Panferov).

0167-2789/$ – see front matter
doi:10.1016/j.physd.2013.02.004

of the Morse potential in $n = 2, 3$. Section 3 introduces Quasi-Morse potentials as fundamental solutions of certain linear PDEs. We will first show that the Quasi-Morse potentials are biologically relevant in essentially the same parameter range as the Morse potentials. Second, we make use of their particular structure to show in our main theorem that flock and mill solutions can be expressed as almost explicit linear combinations of special functions.

Finally, Section 4 is devoted to propose an algorithm to compute the scalar coefficients in the expansion of the flock and mill patterns in terms of the basis functions associated with the Quasi-Morse PDE operators. The strategy uses ideas of constrained optimization methods. We finally compare the results for flocks in 2D and 3D and mills in 2D to particle simulations showing a good agreement. As a conclusion, we demonstrate that the proposed Quasi-Morse potentials are very good alternative to Morse potentials as they share many of their features in the natural parameter range, and at the same time enable explicit computation of the macroscopic density profiles up to numerically determined constants.

2. Swarming: Models and patterns

We will consider a simple second order model for swarming analyzed in [21] consisting of the attraction–repulsion of N interacting self-propelled particles located at $x_i \in \mathbb{R}^n$ with velocities $v_i \in \mathbb{R}^n$ in a host medium with friction, with $n = 1, 2, 3$. Friction is modeled by Rayleigh's law and as a result, an asymptotic speed for the individuals is fixed by the compensation of friction and self-propulsion. More precisely, the time evolution is governed by the equations of motion

$$\begin{aligned} \frac{\mathrm{d}x_i}{\mathrm{d}t} &= v_i, \\ \frac{\mathrm{d}v_i}{\mathrm{d}t} &= \alpha v_i - \beta v_i |v_i|^2 - \nabla_{x_i} \sum_{i \neq j} W(x_i - x_j), \end{aligned} \tag{1}$$

where W is a pairwise interaction potential and α, β are effective values for propulsion and friction forces, see [20,21,25,26] for more discussion. The interaction potential $W : \mathbb{R}^n \times \mathbb{R}^n \to \mathbb{R}$ is assumed to be radially symmetric: $W(x) = U(|x|)$, $x \in \mathbb{R}^n$. The typical asymptotic speed of the individuals is $\sqrt{\alpha/\beta}$. The Morse potential is defined by taking

$$U(r) = -C_A e^{-r/l_A} + C_R e^{-r/l_R},$$

where C_A, C_R are the attractive and repulsive strengths, and l_A, l_R are their respective length scales. We set $V(r) = -\exp(-r/l_A)$, $C = C_R/C_A$, and $l = l_R/l_A$ to obtain

$$U(r) = C_A \left[V(r) - CV\left(\frac{r}{l}\right) \right].$$

The choice of this potential is motivated in [21] for being one of the simplest choices of integrable potentials with easily computable conditions to distinguish the relevant parameters in biological swarms. In fact, it is straightforward to check that in the range $C > 1$ and $l < 1$ the potential $U(r)$ is short-range repulsive and long-range attractive with a unique minimum defining a typical distance between particles. Moreover, in this regime the sign of the integral of the potential:

$$\mathcal{U} := \int_0^\infty W(x)\,\mathrm{d}x = \mathcal{V}(1 - Cl^n) \quad \text{with } \mathcal{V} := \int_0^\infty V(r) r^{n-1}\,\mathrm{d}r < 0, \tag{2}$$

gives a criterion to distinguish between the so-called H-stable and catastrophic regimes. This condition reads as $Cl^n - 1 < 0$ for the catastrophic case in any dimension n, see [21,27]. This property of the potential is important since it is related to the typical patterns emerging in such systems, as classified in [21].

Flocks, where particles tend to form groups, moving with the same velocity, and milling solutions, where rotatory states are formed are of particular interest and are observed in particle and hydrodynamic simulations [21,28] in $n = 2$. Actually, they typically emerge in the large time behavior of the system of particles (1) in the catastrophic regime $Cl^2 < 1$ with $C > 1$ and $l < 1$. In the same range of parameters, randomly chosen initial data lead also to other patterns such as double mills and flocks [21,29]. However mills are not observed in the H-stable regime $Cl^2 > 1$ with $C > 1$ and $l < 1$ while flocks do.

Assuming the weak coupling scaling [30–33] in which the range of interaction is kept fixed and the strength of interaction is divided proportionally between particles, we pass to the rescaled formulation:

$$\begin{aligned} \frac{\mathrm{d}x_i}{\mathrm{d}t} &= v_i, \\ \frac{\mathrm{d}v_i}{\mathrm{d}t} &= v_i(\alpha - \beta |v_i|^2) - \frac{1}{N} \nabla_{x_i} \sum_{i \neq j} U(|x_i - x_j|). \end{aligned}$$

This system has a well-defined limit as $N \to \infty$ which can be expressed as a solution of the corresponding mean-field equation:

$$\partial_t f + v \cdot \nabla_x f + F[\rho] \cdot \nabla_v f + \mathrm{div}\left(\left(\alpha - \beta |v|^2 \right) v f \right) = 0, \tag{3}$$

with

$$\rho(t, x) := \int f(t, x, v)\mathrm{d}v.$$

Here, $f(t, x, v) : \mathbb{R} \times \mathbb{R}^n \times \mathbb{R}^n \to \mathbb{R}$ is the phase-space density, and $\rho(t, x)$ is the averaged (macroscopic) density. The mean-field interaction is given by $F[\rho] = -\nabla_x W \star \rho$.

The limit $N \to \infty$ has been established rigorously for smooth potentials $W \in C_b^2$ in [30–33], in [34,35] for more general models with and without noise, and for more general potentials, with possibly singular behavior at zero, including the Morse potential (2) in the recent result [36].

2.1. Flock and mill states

We are interested in computing certain relevant particular solutions of the Vlasov-like equation for swarming in (3). In fact, we can formally find mono-kinetic solutions of (3) by inserting the ansatz:

$$f(t,x,v) = \rho(t,x)\,\delta(v - u(t,x)), \tag{4}$$

in the weak formulation of (3). The result in [25,29] is that ρ and u should satisfy the following set of hydrodynamic equations:

$$\begin{cases} \dfrac{\partial \rho}{\partial t} + \mathrm{div}_x(\rho u) = 0, \\ \rho\,\dfrac{\partial u}{\partial t} + \rho\,(u\cdot\nabla_x)u = \rho\,(\alpha - \beta|u|^2)u - \rho\,(\nabla_x W \star \rho). \end{cases} \tag{5}$$

Definition 1. A *flock* is a solution f_F of (3) of the form (4) with $\rho(t,x) = \rho_F(x - tu_0)$ and $u(t,x) = u_0$ with $u_0 \in \mathbb{R}^n$ such that $|u_0| = \sqrt{\frac{\alpha}{\beta}}$ and ρ_F a probability measure in $\mathbb{R}^n$.

Obviously, flock solutions are determined by their density profile ρ_F and have the structure of traveling waves in the direction of the velocity vector u_0. It is straightforward to see that, the density of a flock is characterized by the following equation:

Proposition 1. *The function $f_F \geq 0$ is a flock solution if and only if the macroscopic density ρ_F satisfies*

$$\nabla_x W \star \rho_F = 0 \quad \text{on the support of } \rho_F. \tag{6}$$

There are singular solutions to (6) obtained by concentrating all the mass uniformly in a suitable sphere, the so-called Delta rings [29], whose stability for first order models has recently been studied in [37] for certain potentials. Also, there are solutions to (6) given by smooth compactly supported densities for combination of suitable powers in 1D [38,39], for the Morse potential in 1D [24], and for combination of powers when one of them is the repulsive Newtonian potential [40] in 2D. In fact, the set of solutions to (6) can be very complicated even in one dimension [38,39,41] depending on the regularity of the potential.

Let us remark that, since we assume the radial symmetry of the potential, one expects that the density of the flocking solutions to (6) is radially symmetric as well and that it is supported in a ball $B(0,R_F)$ with $R_F > 0$. This is reinforced by the fact that the convolution of radial functions is radial, see Section 2.2 for more precise statements. We will reduce ourselves to find flocking solutions with radial symmetry in the rest of this paper, that is, finding $R_F > 0$ and a radial density $\rho_F(|x|)$ compactly supported in $B(0,R_F)$ satisfying

$$W \star \rho_F = C \quad \text{in } B(0,R_F), \tag{7}$$

for some constant $C \in \mathbb{R}$.

Another interesting type of solutions that spontaneously show up in particle simulations are *mills*, they correspond to motion with the velocity field of a point vortex:

$$u_M(x) = \pm\sqrt{\frac{\alpha}{\beta}}\,\frac{x^\perp}{|x|}, \tag{8}$$

where $x = (x_1,x_2)$, $x^\perp = (-x_2,x_1)$, such that $\rho_M(|x|)$ is a radially symmetric stationary solution to (5).

Definition 2. A *mill* is a solution f_M of (3) of the form:

$$f_M(t,x,v) = \rho_M(x)\,\delta(v - u_M(x)),$$

with u_M given by (8) and ρ_M radially symmetric.

As shown in [20,29,28], mill solutions can also be characterized as:

Proposition 2. *$\rho_M(x)$ is a mill density if and only if*

$$\nabla_x\left[W \star \rho - \frac{\alpha}{\beta}\log|x|\right] = 0, \quad \text{on the support of } \rho.$$

As discussed above, one can obtain singular mill solutions by concentrating all particles in a ring [29]. However, we will search for radial solutions supported in an annulus $B(R_m,R_M)$ with $0 < R_m < R_M$, and therefore, mill radial solutions supported in $B(R_m,R_M)$ are characterized by

$$W \star \rho_M = D + \frac{\alpha}{\beta}\log|x| \quad \text{in } B(R_m,R_M), \tag{9}$$

for some constant $D \in \mathbb{R}$. In the following, the subindex x in differential operators is dropped since we only deal with x-dependent functions.

2.2. Convolution of radial functions

Since we want to find particular radial solutions to flocks (7) and mills (9), we need suitable expressions of the convolution of two radial functions in $n = 2, 3$. Given any radial density $\rho(|x|)$, then the convolution term rewrites:

$$(W \star \rho)(x) = \int_{\mathbb{R}^n} W(x-y)\rho(|y|)\mathrm{d}y = \int_0^\infty \int_{\partial B(0,1)} W(x - s\omega)\rho(s)s^{n-1}\mathrm{d}\omega\mathrm{d}s$$

which is *not* a convolution in $r = |x|$ anymore, but rather is given by an integral operator of the following form:

$$(W \star \rho)(r) = \int_{\mathbb{R}^+} \Psi(r,s)\rho(s)\mathrm{d}s$$

with

$$\Psi(r,s) = s^{n-1} \int_{\partial B(0,1)} U(|re_1 - s\omega|)\mathrm{d}\omega.$$

Expressing it in polar ($n = 2$) or spherical ($n = 3$) coordinates, we get the functions

$$\Psi(r,s) = s \int_0^{2\pi} U\left(\sqrt{r^2 - 2rs\cos\theta + s^2}\right)\mathrm{d}\theta \tag{10}$$

for $n = 2$ and

$$\begin{aligned}\Psi(r,s) &= s^2 \int_0^{2\pi}\int_0^{\pi} U(|re_1 - s\omega(\theta,\nu)|)\,\sin\nu\,\mathrm{d}\nu\,\mathrm{d}\theta \\ &= 2\pi s^2 \int_0^{\pi} U\left(\sqrt{r^2 - 2rs\cos\nu + s^2}\right)\,\sin\nu\,\mathrm{d}\nu,\end{aligned} \tag{11}$$

with $\omega(\theta,\nu) = (\cos\nu, \sin\nu\cos\theta, \sin\nu\sin\theta)$ for $n = 3$.

3. Quasi-Morse potentials and their explicit solvability

In this section, we define Quasi-Morse potentials for $n = 1, 2, 3$ and discuss their properties. These Quasi-Morse potentials will yield biologically relevant shapes similar to the Morse potentials. We show that flock and mill solutions in the natural parameter range, see Figs. 4 and 8(d) for precise statements, can be computed explicitly up to numerically determined constants.

3.1. Definition and comparison

Definition 3. Let $V : \mathbb{R}^+ \to \mathbb{R}$ denote the radially symmetric solution of the n-dimensional *screened Poisson equation* $\Delta u - k^2 u = \delta_0$, for a given $k > 0$, that vanishes at infinity. Let $C, l, \lambda \in \mathbb{R}$ be further positive parameters. Then we say that, $U(|x|)$ is the *n-dimensional Quasi-Morse potential* if

$$U(r) := \lambda\left(V(r) - C\,V\left(\frac{r}{l}\right)\right).$$

Using the radially symmetric ansatz, the screened Poisson equation reduces to a second-order ordinary differential equation dependent on the space dimension. For relevant $n = 1, 2, 3$ this ODE possesses two linearly independent solutions. We therefore have

Corollary 1. *Quasi-Morse potentials for $n = 1, 2, 3$ are well-defined and constructed from the following fundamental solution:*

$$\begin{cases} n = 1 : V(r) = -\dfrac{1}{k}e^{-kr} \\ n = 2 : V(r) = -\dfrac{1}{2\pi}K_0(kr) \\ n = 3 : V(r) = -\dfrac{1}{4\pi}\dfrac{e^{-kr}}{r} \end{cases} \tag{12}$$

where K_0 is the modified Bessel function of second kind. For $n = 1$, the Quasi-Morse potential equals the Morse potential.

We illustrate the Quasi-Morse potential in comparison to the Morse potential for $n = 2$ with parameters $C = 10/9$ and $l = 0.75$ in Fig. 1. Both potentials could be used to model the biologically motivated interplay between short-range repulsion and long-range attraction, and there is no clear reason to prefer one over the other. A significant difference is the behavior at zero, where Morse is finite and Quasi-Morse

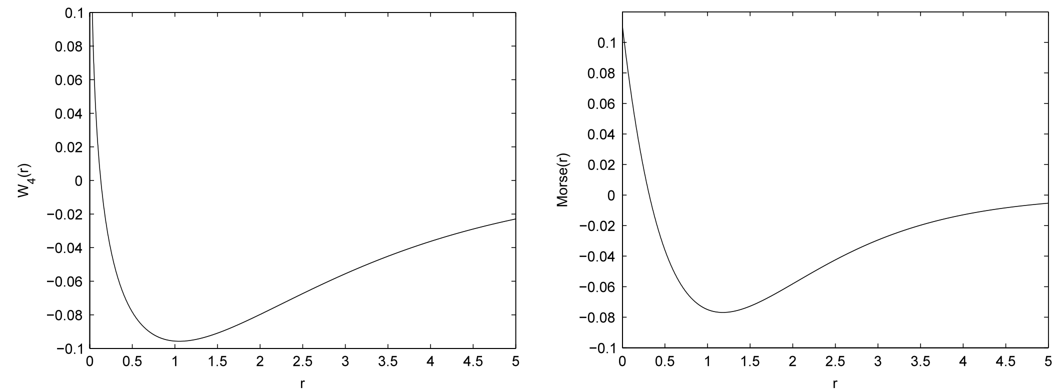

(a) Quasi-Morse potential. (b) Morse potential.

Fig. 1. Comparison of potentials: Both yield the biologically relevant shape of short-range repulsion and long-range attraction (Quasi-Morse: $n = 2$, $C = \frac{10}{9}$, $l = 0.75$, $k = \frac{1}{2}$, $\lambda = 4$, Morse: $C = \frac{10}{9}$, $l = 0.75$, $\lambda = 2$).

is singular though locally integrable for $n > 1$, which are the dimensions we aim to study. The parameter dependence of catastrophic regimes is inherited from the Morse potential as summarized in the next result, whose proof is given in an Appendix.

Corollary 2. *The function $U(r)$ has a unique minimum if and only if $l < 1, Cl^{n-2} > 1$. Furthermore, the Quasi-Morse potential $U(|x|)$ is catastrophic if $Cl^n < 1$.*

Remark 1. We first emphasize that, the global minimum of U corresponds to the biologically relevant scenario of short-range repulsion and long-range attraction, as for the standard Morse potential. Concerning the H-stability of the Quasi-Morse potentials, we remark that the inverse Fourier transform of $U(r)$ for $k = 1$ reads

$$\check{U}(|\xi|) = \frac{Cl^n - 1 + l^2(Cl^{n-2} - 1)|\xi|^2}{(1 + |\xi|^2)(1 + l^2\,|\xi|^2)}$$

which is positive if $Cl^n > 1$ and $Cl^{n-2} > 1$. This indicates the H-stability, but the criteria developed in [27] do not apply directly, since $\check{U}(|\xi|)$ is not integrable in dimensions $n = 2, 3$. However, our numerical findings presented in the following sections will suggest H-stability for the configurations $l < 1, Cl^{n-2} > 1,\ Cl^n > 1$. This corresponds to potentials having a unique minimum and a positive n-dimensional integral.

Next, we mention the influence of the free scaling parameter k and show that, any potential shape can be normalized to $k = 1$, see Appendix. The following results are given without proof which follows easily by a change of variables from the convolution form in radial coordinates (10) and (11) in Section 2.2.

Corollary 3. *Let ρ be the flock (resp. mill) solution setting $k = 1$ with support $B(0, R)$ (resp. $B(R_m, R_M)$), then the transformed solution $\tilde{\rho}$ for the potential scaled to $k = \tilde{k} \neq 1$ is given by*

$$\begin{cases} \text{flock} : \tilde{\rho}(x) = \tilde{k}^n \rho(\tilde{k}x), & \operatorname{supp}(\tilde{\rho}) = B\left(0, \dfrac{R}{\tilde{k}}\right) \\ \text{mill} : \tilde{\rho}(x) = \tilde{k}^2 \rho(\tilde{k}x), & \operatorname{supp}(\tilde{\rho}) = B\left(\dfrac{R_m}{\tilde{k}}, \dfrac{R_M}{\tilde{k}}\right). \end{cases}$$

Denoting $\tilde{U}(r) := U(\tilde{k}r)$, $\tilde{W}(x) = \tilde{U}(|x|)$, we have $\tilde{W} \star \tilde{\rho} = W \star \rho = C\tilde{k}^{2-n}$ for flocks, and $\tilde{W} \star \tilde{\rho} = W \star \rho + \frac{\alpha}{\lambda\beta} \log(\tilde{k})$ for mill solutions.

3.2. Explicit solvability

In this section, we show how to solve almost explicitly the integral equations for flock and mill profiles with the Quasi-Morse potential. The exact problem to solve for any potential W is to find a density ρ and its support such that

$$(W \star \rho)(r) = s(r) \quad \text{on } \operatorname{supp}(\rho) \tag{13}$$

with some radial $s(r)$ on $\operatorname{supp}(\rho) = B(R_m, R_M)$, $0 \le R_m < R_M$. Solving (13) generally implies inverting the integral operator, a task that is complicated by the fact that the support is unknown. Even if this is numerically achievable, we will not learn anything about the structure of the solutions. For the Quasi-Morse potential, we take advantage of the differential operators behind its construction, to avoid the inversion of (13) and to give an almost explicit expression of its solution in terms of special functions. This strategy was already done in [24] in the one dimensional case, where Morse and Quasi-Morse potentials coincide. In this section, we pursue a similar strategy for the Quasi-Morse potential in $n = 2, 3$.

We begin our discussion reminding the radially symmetric fundamental system associated with some operators, which will be needed henceforth.

Remark 2. The n-dimensional *Helmholtz equation* reads $\Delta u + k^2 u = 0$ in $\mathbb{R}^n$. Its fundamental system of radially symmetric solutions $\{\varphi_1, \varphi_2\}$ is associated to a second-order ordinary differential equation (in radial coordinates for $n = 2, 3$) and given below, together with the fundamental system of the already mentioned screened Poisson equations $\{\psi_1, \psi_2\}$:

Helmh.	φ_1	φ_2	s.Poiss.	ψ_1	ψ_2
$n = 1$	$\frac{1}{2k}\sin(kr)$	$-\frac{1}{2k}\cos(kr)$	$n = 1$	$\frac{1}{2k}e^{kr}$	$-\frac{1}{2k}e^{-kr}$
$n = 2$	$-\frac{1}{2\pi}J_0(kr)$	$\frac{1}{2\pi}Y_0(kr)$	$n = 2$	$\frac{1}{2\pi}I_0(kr)$	$-\frac{1}{2\pi}K_0(kr)$
$n = 3$	$\frac{1}{4\pi}\frac{\sin(kr)}{r}$	$-\frac{1}{4\pi}\frac{\cos(kr)}{r}$	$n = 3$	$\frac{1}{4\pi}\frac{e^{kr}}{r}$	$-\frac{1}{4\pi}\frac{e^{-kr}}{r}$

Here, J_0 and Y_0 are the Bessel functions of the first and second kind respectively, while I_0 and K_0 are the modified Bessel functions of the first and second kind respectively.

We continue with a simple computation related to the local properties of our potential.

Lemma 1. *Let V be the fundamental solution of the screened Poisson equation. Then*

$$\Delta_x \left(V\left(\frac{x}{l}\right)\right) = \frac{k^2}{l^2}V + l^{n-2}\delta_0.$$

Proof. Let ξ be a test function. Then by change of variables

$$\begin{aligned}\int_{\mathbb{R}^n} \Delta_x \left(V\left(\frac{x}{l}\right)\right)\xi(x)\,\mathrm{d}x &= \frac{1}{l^2}\int_{\mathbb{R}^n}(\Delta V)\left(\frac{x}{l}\right)\xi(x)\mathrm{d}x = \frac{1}{l^2}\int_{\mathbb{R}^n}\Delta V(z)\xi(lz)l^n\mathrm{d}z \\ &= \frac{l^n}{l^2}\left(\int_{\mathbb{R}^n}k^2V(z)\xi(lz)\mathrm{d}z + \xi(0)\right) \\ &= \frac{1}{l^2}\int_{\mathbb{R}^n}k^2V(z)\xi(lz)l^n\mathrm{d}z + l^{n-2}\xi(0) \\ &= \frac{k^2}{l^2}\int_{\mathbb{R}^n}V\left(\frac{x}{l}\right)\xi(x)\mathrm{d}x + l^2\xi(0)\end{aligned}$$

leading to the weak formulation of the claim. □

Now, we can state the main result of this section.

Theorem 1. *Assume there exists a solution of $(W \star \rho)(r) = s(r)$ on $\mathrm{supp}(\rho)$ with W being the Quasi-Morse potential and $\mathrm{supp}(\rho) = B(0, R_F)$, $s(r) = D$ for flocks, or $\mathrm{supp}(\rho) = B(R_m, R_M)$, $s(r) = D + \frac{\alpha}{\beta}\log(r)$ for mills respectively. Then ρ has to be of the following form on $\mathrm{supp}\rho$:*

$n = 2$:	Flock	$A > 0$	$\rho_F = \mu_1 J_0(ar) + \mu_2$
		$A = 0$	$\rho_F = \mu_1 r^2 + \mu_2$
		$A < 0$	$\rho_F = \mu_1 I_0(ar) + \mu_2$
	Mill	$A > 0$	$\rho_M = \rho_{\text{inhom}} + \mu_1 J_0(ar) + \mu_2 Y_0(ar) + \mu_3$
		$A = 0$	$\rho_M = \frac{\alpha}{\beta}\frac{k^4}{4\lambda l^2(1-C)}r^2(\log(r)-1)+\mu_1 r^2+\mu_2\log(r)+\mu_3$
		$A < 0$	$\rho_M = \rho_{\text{inhom}} + \mu_1 I_0(-ar) + \mu_2 \cdot K_0(ar) + \mu_3$
$n = 3$:	Flock	$A > 0$	$\rho_F = \mu_1 \sin(ar)\frac{1}{r} + \mu_2$
		$A = 0$	$\rho_F = \mu_1 r^2 + \mu_2$
		$A < 0$	$\rho_F = \mu_1 \sinh(ar)\frac{1}{r} + \mu_2$

with $A = k^2\frac{Cl^n - 1}{l^2 - Cl^n}$, $a^2 = |A|$, and ρ satisfying $\rho > 0$, $\int \rho\mathrm{d}x = 1$.

Proof. Let us define the operators $\mathcal{L}_1 := \Delta - k^2 I$, $\mathcal{L}_2 := \Delta - \frac{k^2}{l^2} I$. We apply both operators to the equation and obtain

$$\begin{aligned}\mathcal{L}_2\mathcal{L}_1(W\star\rho) &= (\mathcal{L}_2\mathcal{L}_1 W)\star\rho = \lambda\left(-C\,\mathcal{L}_1\mathcal{L}_2 V\left(\frac{r}{l}\right) + \mathcal{L}_2\mathcal{L}_1 V(r)\right)\star\rho\\ &= \lambda\left(-Cl^{n-2}\Delta\delta + Ck^2 l^{n-2}\delta + \Delta\delta - \frac{k^2}{l^2}\delta\right)\star\rho\\ &= \lambda(1-Cl^{n-2})\Delta\rho + \lambda\left(Ck^2l^{n-2} - \frac{k^2}{l^2}\right)\rho = \mathcal{L}_2\mathcal{L}_1 s\end{aligned}$$

using Lemma 1. Hence, ρ should satisfy the following equation in its support:

$$\Delta\rho \pm a^2\rho = \frac{1}{\lambda}\frac{1}{1-Cl^{n-2}}\mathcal{L}_2\mathcal{L}_1 s, \tag{14}$$

with $a^2 = |A|$ and

$$A = \frac{Ck^2l^{n-2} - \frac{k^2}{l^2}}{1-Cl^{n-2}} = k^2\frac{Cl^n - 1}{l^2 - Cl^n},$$

resulting in the Helmholtz equation for $A > 0$, the screened Poisson equation for $A < 0$ and the Poisson equation for $A = 0$ with radially symmetric inhomogeneous right-hand side. Therefore, the solution to (14) writes as a general solution of the homogeneous problem given by a linear combination of the fundamental system in Remark 2 plus a particular solution of the inhomogeneous problem.

The right-hand side of (14) depends on the type of solution we wish to compute. For flocks in any dimension, $s(r)$ is a constant function, and then we have $\frac{1}{\lambda(1-Cl^{n-2})}\mathcal{L}_2\mathcal{L}_1 s(r) = \tilde{D}$. Therefore, the inhomogeneous solution of (14) for $A \neq 0$ with unknown constant right-hand side $\tilde{D}$ is

$$\rho_{\text{inhom},A}(r) = \frac{\tilde{D}}{A}\mathbb{1}_{\text{supp }\rho}.$$

For mills and $n = 2$, we have $s(r) = D + \frac{\alpha}{\beta}\log(r)$ to obtain

$$\frac{1}{\lambda(1-C)}\mathcal{L}_2\mathcal{L}_1\left[D + \frac{\alpha}{\beta}\log(r)\right] = \frac{k^4}{\lambda l^2(1-C)}\frac{\alpha}{\beta}\log(r) + \tilde{D} \tag{15}$$

since $\log(r)$ is the fundamental solution of the Laplacian and its Dirac delta disappears and we look for mill solutions on an annulus (see Section 2, (9)). Therefore, the inhomogeneous solution of (14) with right-hand side (15) can also be written explicitly. Again since $\log(r)$ is a fundamental solution of the Laplacian and the support of the solution is assumed not to contain the origin, it states

$$\rho_{\text{inhom},A}(r) = \frac{k^4}{\lambda a^2 l^2(1-C)}\frac{\alpha}{\beta}\log(r) + \frac{\tilde{D}}{A} \quad \text{on supp } \rho \text{ for } A \neq 0.$$

Finally, in case $A = 0$, the inhomogeneous solution for the flock case is

$$\rho_{\text{inhom},0} = \begin{cases}\frac{1}{4}\tilde{D}r^2, & n = 2\\ \frac{1}{6}\tilde{D}r^2, & n = 3,\end{cases}$$

whereas in the mill case it reads

$$\rho_{\text{inhom},0} = \frac{\alpha}{\beta}\frac{k^4}{4\lambda l^2(1-C)}r^2(\log(r) - 1) + \frac{1}{4}\tilde{D}r^2$$

by using the fundamental solution of the Laplace operator. Putting together the inhomogeneous solution with the homogeneous part leads to the claim of the theorem. For flocks, the space of candidate solutions is of lower dimension, since singularities at the origin are excluded. □

The coefficients (μ_1, μ_2) or (μ_1, μ_2, μ_3) have to be computed numerically under the constraint that the solution has to be non-negative, has to contain unit mass, and has to solve the original equation (13), but only on its own support which is a priori unknown. To achieve this, we now need only to evaluate the convolution integral in (13) in a constrained optimization method rather than its inversion.

Remark 3. Finally, we show that the radius of the support R and the constants (μ_1, μ_2) are connected by an explicit nonlinear identity in the particular case of 3D flocks. By plugging the definition of the Quasi-Morse potential in 3D (12) into (11), then

$$\Psi(r,s) = \frac{\lambda s}{2rk}\left(Cl^2 e^{-\frac{k}{l}|r-s|} - e^{-k|r-s|} - Cl^2 e^{-\frac{k}{l}(r+s)} + e^{-k(r+s)}\right).$$

By looking up in the table of Theorem 1, we have the explicit expression of $\rho_F(r)$ for flocks with $A > 0$ and $n = 3$. Straightforward computations lead to

$$\int_0^R \Psi(r,s)\rho_F(s)ds - \frac{\lambda\mu_2}{k^2}(Cl^3-1) = \frac{\lambda Cl^3}{k^3(k^2+a^2l^2)}\Lambda(C,l)e^{-\frac{k}{l}R}\frac{\sinh\left(\frac{k}{l}r\right)}{r} - \frac{\lambda}{k^3(k^2+a^2)}\Lambda(1,1)e^{-kR}\frac{\sinh kr}{r}$$

where $A = a^2$ was used, and with

$$\Lambda(C,l) = \mu_1 k^2 al\cos Ra + \mu_2 ka^2l^2R + l^3\mu_2a^2 + \mu_2 lk^2 + \mu_1k^3\sin Ra + \mu_2k^3R.$$

Therefore, the existence of a flock solution is equivalent to the conditions $\Lambda(C,l) = 0$ and $\Lambda(1,1) = 0$, or equivalently

$$\begin{pmatrix} k^2al\cos Ra + k^3\sin Ra & ka^2l^2R + a^2l^3 + lk^2 + k^3R \\ k^2a\cos Ra + k^3\sin Ra & ka^2R + a^2 + k^2 + k^3R \end{pmatrix}\begin{pmatrix}\mu_1\\ \mu_2\end{pmatrix} = \begin{pmatrix}0\\0\end{pmatrix}.$$

A necessary condition (ρ_F can still be negative) is that, the determinant of the matrix on the left hand side is zero, i.e., the existence of the solution of the nonlinear equation for R

$$\tan Ra = \frac{a}{k}\frac{k^3R - a^2(l^2+l+klR)}{ka^2R + a^2(l^2+l+1)+k^2}.$$

So that, for flock solutions in 3D we only need to check for radii verifying this last identity.

In the next section, we will show an algorithm to solve this problem and present the numerical results.

4. Numerical investigations

Theorem 1 shows that, solutions of (13) are solutions of (14) with the constraints of positivity, unit mass, and compact support on an annulus. Therefore, we now propose an algorithm that numerically determines the support and linear factors μ_i of the stationary flock and mill solution. We will also present results which are compared to particle simulations.

4.1. The algorithm

Let parameters $n, C, l, k, \alpha, \beta$ be fixed and ρ_{hom} denote the homogeneous solution dependent on dimension as in Theorem 1. In search for the support of the solution, we set the parameter $R_{\max}$ as an upper boundary on the support size the algorithms shall consider. We can ensure that, this is no restriction to the final result by setting $R_{\max}$ large compared to the characteristic shape of the potential. Furthermore, denote Δr a discretization parameter and $\{r_0,\dots,r_N\}$ an equidistant discretization of a chosen support $\mathrm{supp}(\rho)$, with $r_{i+1} - r_i = \Delta r$. Numerical approximations of functions $F(r)$ on the discrete radial grid are denoted with $\bar{F}$. Our first algorithm determines the best possible solution for *one particularly chosen* support $B(R_l, R_r)$. We aim to find linear coefficients (μ_1, μ_2) (or (μ_1,μ_2,μ_3) respectively), which solve the integral equation (13) the best possible way. Non-negativity and unit mass of ρ are hard constraints, whereas the deviation $W \star \rho - s$ serves as the objective function the coefficients shall minimize.

Algorithm 1 (*For Flocks*).

Input : fixed support $B(0, R_r)$
- For convolving functions with the potential, compute a matrix H s.t. $\overline{W\star\rho} = H\bar{\rho}$ according to Section 2.2.
- Evaluate the convolution of the basis functions ρ_{hom} and 1 on $\mathrm{supp}\rho$:

$$g^1 := H\bar{\rho}_{\text{hom}},\, g^2 := H\,\bar{1}.$$

- To fit the right hand side $s(r) = D$ on the support, we chose coefficients such that $s(r) = D$ at the two end points r_1, r_N. That is, solving

$$\begin{pmatrix} g_1^1 & g_1^2 \\ g_N^1 & g_N^2\end{pmatrix}\mu_{\text{const}} = \begin{pmatrix}1\\1\end{pmatrix}$$

setting $D = 1$ temporarily.
- By linearity of H, we set $\bar{\rho} := \frac{1}{M}(\mu_{\text{const},1}\rho_{\text{hom}} + \mu_{\text{const},2})$ with M normalizing total mass.
- Since we have only ensured (13) to hold at two points, we measure deviation of $H\bar{\rho}$ from $s(r)$ (here, an arbitrary constant) on the whole support as

$$e := \frac{1}{R_r}\int\left[H\bar{\rho} - \frac{1}{R_r}\int H\bar{\rho}\,\mathrm{d}\bar{r}\right]\mathrm{d}\bar{r}.$$

Output : $e, \bar{\rho}, \bar{s}$ if $\bar{\rho} \geq 0$, error message if $\bar{\rho} \ngeq 0$.

For the case of mills, we proceed analogously, but we have to take into account the fixed inhomogeneous solution and three basis functions.

Algorithm 2 (*For Mills*).

Input : fixed support $B(R_m, R_M)$
- For convolving functions with the potential, compute a matrix H s.t. $\overline{W \star \rho} = H\bar{\rho}$ according to Section 2.2.
- Evaluate the convolution of the fixed inhomogeneous part $\rho_{\text{inhom},A}$ on suppρ and set $\bar{s}_{\text{inhom}} := H\bar{\rho}_{\text{inhom},A}$.
- Define the remainder of the right-hand side as $\bar{s}_{\text{rem}} := \bar{s} - \bar{s}_{\text{inhom}}$, which has to be fitted by the convolution of the basis functions.
- To do so, evaluate $J_0(ar)$, $Y_0(ar)$ and 1 on suppρ:

$$g^1 := H\bar{J_0},\, g^2 := H\bar{Y_0},\, g^3 := H\bar{1}.$$

- Giving three basis functions, we pick three points r_1, r_j with $j = \lfloor N/2 \rfloor$, r_N and interpolate both the remainder $\bar{s}_{\text{rem}}$ and the free constant, which is temporarily set to 1. We solve

$$\begin{pmatrix} g_1^1 & g_1^2 & g_1^3 \\ g_j^1 & g_j^2 & g_j^3 \\ g_N^1 & g_N^2 & g_N^3 \end{pmatrix} \mu_{\text{rem}} = \begin{pmatrix} \bar{s}_{\text{rem},1} \\ \bar{s}_{\text{rem},j} \\ \bar{s}_{\text{rem},N} \end{pmatrix}$$

$$\begin{pmatrix} g_1^1 & g_1^2 & g_1^3 \\ g_j^1 & g_j^2 & g_j^3 \\ g_N^1 & g_N^2 & g_N^3 \end{pmatrix} \mu_{\text{const}} = \begin{pmatrix} 1 \\ 1 \\ 1 \end{pmatrix}$$

- By linearity of H, we set $\bar{\rho}_{\text{rem}} := \mu_{\text{rem},1}\bar{J_0} + \mu_{\text{rem},2}\bar{Y_0} + \mu_{\text{rem},3}$ and

$$\bar{\rho}_{\text{const}} := \mu_{\text{const},1}\bar{J_0} + \mu_{\text{const},2}\bar{Y_0} + \mu_{\text{const},3}.$$

- Our last degree of freedom is the free constant on the right hand side $s(r)$, which we use to normalize mass. The candidate density is

$$\bar{\rho} := \bar{\rho}_{\text{inhom},A} + \bar{\rho}_{\text{rem}} + \gamma\,\bar{\rho}_{\text{const}} \text{ with } \gamma := \frac{1 - m(\bar{\rho}_{\text{rem}}) - m(\bar{\rho}_{\text{inhom},A})}{m(\bar{\rho}_{\text{const}})}.$$

- We penalize deviation of $H\bar{\rho}$ from $s(r)$ on the entire support as

$$e_1 := \frac{1}{R_M - R_m} \int \left[H\bar{\rho} - \bar{s} - \frac{1}{R_M - R_m} \int (H\bar{\rho} - \bar{s})\mathrm{d}\bar{r} \right] \mathrm{d}\bar{r}.$$

- Second, since $s(r)$ is concave, we penalize numerical convexity of $\bar{s}$ by

$$e_2 := \int \chi_{[\bar{s}''>0]}\,\bar{s}\mathrm{d}\bar{r}$$

The total penalty value is the sum of e_1, e_2.

Output : $e = e_1 + e_2$, $\bar{\rho}$, $\bar{s}$ if $\bar{\rho} \geq 0$

Now, we search the minimizer of the error function e over a test set of supports, given by the pre-defined discretization Δr_1 and maximal support size. Repeating Algorithm 1 over the set of test supports provides a minimizer of the penalty function. For flocks, the number of tested supports is $\approx \frac{R_{\max}}{\Delta r_1}$, for mills $\approx \frac{1}{2}\left(\frac{R_{\max}}{\Delta r_1}\right)^2$. To enhance the speed of numerical computation, we first compute a solution based on a coarser discretization length $\Delta r_2 = m\Delta_{r_1}$ for some integer m. Then, the obtained minimizer is used as the center of a local refinement search with a fine discretization length, as illustrated in Algorithm 3:

Algorithm 3.

- Choose a coarse grid size Δr_2 such that an iteration of Algorithm 1 over all test supports is reasonably fast and, as a solution, obtain the support $B(0, \tilde{R}_F)$ (or $B(\tilde{R}_m, \tilde{R}_M)$) for mills.
- Vary this support locally up to a fixed parameter c with a fine discretization $\Delta r_1 \ll \Delta r_2$, re-run Algorithm 1 restricted on $|R_F - \tilde{R}_F| \leq c$ ($|R_m - \tilde{R}_m| \leq c$, $|R_M - \tilde{R}_M| \leq c$ for mills).
- Obtain the minimizing results supp(ρ), $\bar{\rho}$, $\bar{s}$ and e.

Naturally, the matrix H is not recomputed in every iteration but constructed once for the largest support and inherited. The choice to fix a functional equality on the points which are most left, most right and for mills central on the chosen support is arbitrary. We say that, no compact solutions are found in our computations, if our algorithms deliver $R_{\max}$ as the error minimizer, no matter of its value. The convergence of the algorithm for $\Delta r \to 0$ if compact solutions are found will be demonstrated together with the results of the next subsection.

4.2. Flocks in 2D

We start our presentation of numerical results with the aligned flock in two dimensions. Our standard example is the configuration $C = \frac{10}{9}$, $l = 0.75$, $k = \frac{1}{2}$ as in Fig. 1. The stationary aligned flock state is independent of λ, α, β, yet emergence of flocks in particle simulations

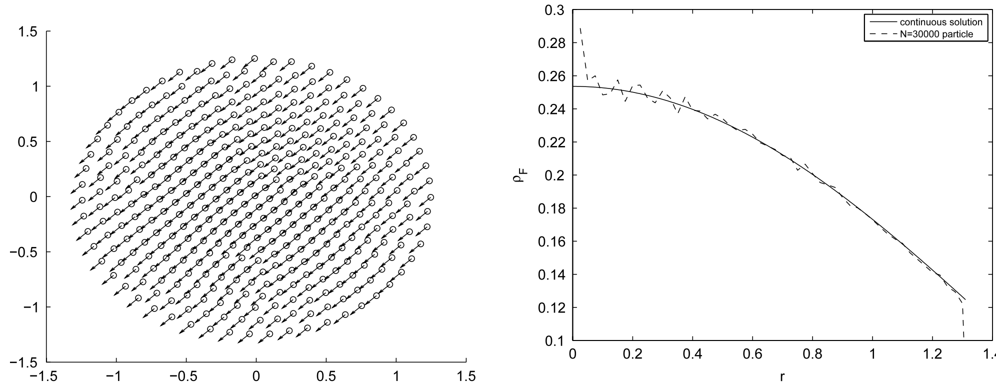

(a) Flock emerged in a particle simulation with $N = 400$ particles.

(b) Radial flock density: Continuous result vs. empirical density ($N = 30\,000$ particles).

Fig. 2. Two-dimensional aligned flocks emerge for the Quasi-Morse potential. The resulting continuous radial density of Algorithms 1 and 3 matches the empirical distribution obtained from particle simulations. The stationary flock has the form $\rho_F = \mu_1 J_0(ar) + \mu_2$ with, in this case, $\mu_1 \approx 0.2356$, $\mu_2 \approx 0.018$, $A = 1.5$, $R_F \approx 1.31$. (Quasi-Morse potential parameters in use are $C = \frac{10}{9}$, $l = 0.75$, $k = \frac{1}{2}$.)

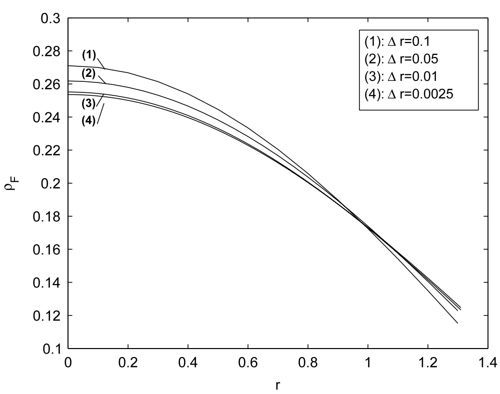

(a) Continuous solution ρ_F for varying Δr.

Δr	error e	computation time
0.1	3.54e-05	0.76s
0.05	1.36e-05	2.85s
0.01	3.99e-06	69.1s
0.0025	9.97e-07	1125s

(b) Minimal error value and computation times.

Fig. 3. Algorithms 1, 3 converge as $\Delta r \to 0$ if a compactly supported flock solution exists. Four resulting densities are shown for $\Delta r \in \{0.1, 0.05, 0.01, 0.0025\}$ together with the minimal error value of the algorithm and the corresponding computation time.

depends on these parameters and suitable initial conditions. An exemplary convenient choice is $\alpha = 1$, $\beta = 5$, $\lambda \in \{100, 1000\}$. The observed flock of aligned particles is illustrated in Fig. 2(a) for $N = 400$ particles. In Fig. 2(b), the result of our investigations is compared to the empirical radial density obtained from a particle simulation with $N = 30\,000$ agents. The empirical radial density is obtained by collecting particles in radial bins and dividing by the Jacobian of the radial transformation. We see that, the continuous solution matches the particle density and convergence is expected as $N \to \infty$. While the numerical cost of full particle simulations is at least $\mathcal{O}(N^2)$, the computational effort of the presented method scales quadratically with Δr, as illustrated in Fig. 3(b). In Fig. 3(a) we show the convergence of our algorithms as $\Delta r \to 0$. One observes that, the support is estimated well for coarse grid sizes, whereas the correct radial density is established with finer discretizations. The minimal error values of Algorithms 1, 3 are listed in Fig. 3(b). The advantages of the presented solution are continuity, dramatic reduction of the numerical cost, fast convergence, and an explicit expression of the radial density as, in this example, a combination of Bessel's J-function and a constant.

Concerning the potential parameters, the area of relevant short-term repulsion and long-range attraction shapes divides into two subregions based on the results of Section 3, as illustrated in Fig. 4: In region I with $C > 1,\ l < 1,\ Cl^2 < 1$, the potential is catastrophic, $A > 0$ (from Theorem 1) and compactly supported continuous flock solutions are found. In region II with $C > 1,\ l < 1,\ Cl^2 < 1, A < 0$ (from Theorem 1), and no compactly supported solutions can be found. No solution of the algorithm indicates H-stability since in this case particle simulations do show flocks, whose support diverges when $N \to \infty$. The presented method faces numerical difficulties for catastrophic potentials $A > 0$ with $Cl^2 \approx 1$, where it eventually breaks down not converging to a compactly supported flock. Similarly, particle simulations are not fully reliable in this limiting cases. However, thanks to our computation in Section 3 we are able to consider the exact separatrix case $Cl^2 = 1,\ C > 1,\ l < 1, A = 0$: Here, no compact solutions are found. Our numerical findings are illustrated in Fig. 4. We emphasize that based on the reported simulations, we conjecture that compactly supported flock solutions exist only in the catastrophic regime, $A > 0$.

4.3. Mills in 2D

The Quasi-Morse potential is able to produce rotating mill states in particle simulations, just as the original Morse potential. We choose the same configuration as in Section 4.2 with $\lambda = 100$ and show the mill emerging from a particle simulation in Fig. 5(a). The resulting mill solution of our algorithms is illustrated in Fig. 2(b), together with a comparison to an empirical density from a particle mill with $N = 16\,000$ agents. Again, our result is confirmed by the particle simulation and support as well as the density shape agree perfectly. The stationary

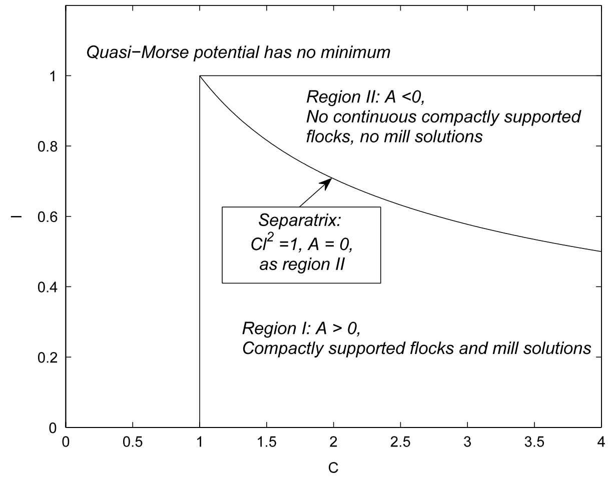

Fig. 4. Numerical phase diagram of the Quasi-Morse potential in 2D: The biologically relevant scenarios decompose into two subregions. Region I: $A > 0$, continuous compactly supported flocks. Region II: $A \leq 0$, no compactly supported continuous solutions, flocks only emerge on particle level. The same division of regions applies to the mill solutions.

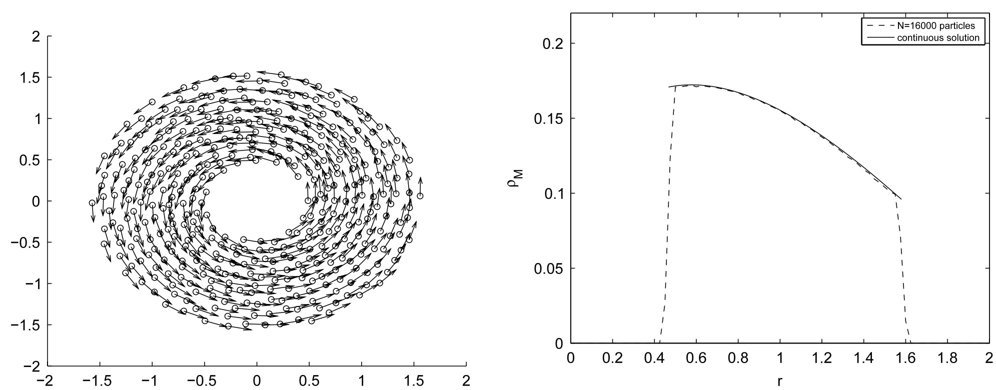

(a) Mill emerged in a particle simulation with $N = 400$ particles.

(b) Radial mill density: Continuous result vs. empirical measure ($N = 16\,000$ particles).

Fig. 5. Rotating mills emerge for the Quasi-Morse potential. As for flocks, the resulting radial density of Algorithms 1, 3 matches the empirical distribution obtained from particle simulations. The mill solution has the form $\rho_M = \rho_{\text{inhom},A} + \mu_1 J_0(ar) + \mu_2 Y_0(ar) + \mu_3$ with, in this case, $\mu_1 \approx 0.1708$, $\mu_2 \approx 0.0468$, $\mu_3 = 0.0320$, $A = 1.5$, $\text{supp}_{\rho_M} \approx B(0.47, 1.57)$. (Quasi-Morse potential parameters in use are $C = \frac{10}{9}$, $l = 0.75$, $k = \frac{1}{2}$, others are $\alpha = 1$, $\beta = 5$, $\lambda = 100$.)

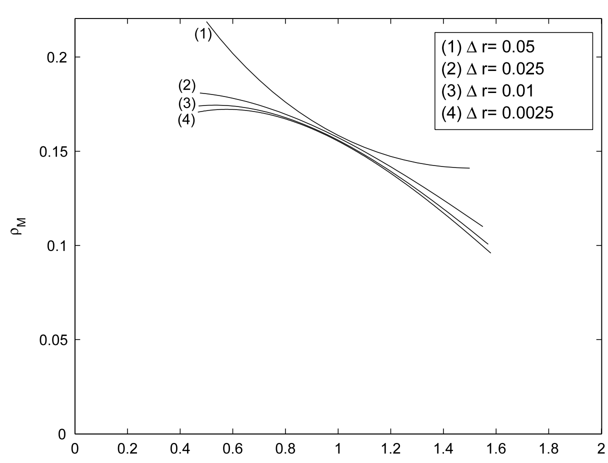

Fig. 6. Algorithms 1, 3 converge for the mill case as $\Delta r \to 0$.

rotating mill is a weighted sum of Bessel's J and Y functions, the inhomogeneity ρ_{hom} and a constant. The convergence of Algorithms 1, 3 in the mill case is shown in Fig. 6. As for flocks, the computational costs are minimal compared to a full particle simulation. For the existence of compactly supported mill solutions, the parameter diagram on Fig. 4 applies just as for flocks. In region I, continuous solutions can be found, whereas in region II and the separatrix $Cl^2 = 1$ no such mills can be found. In particle simulations, we there see either a crystal-like

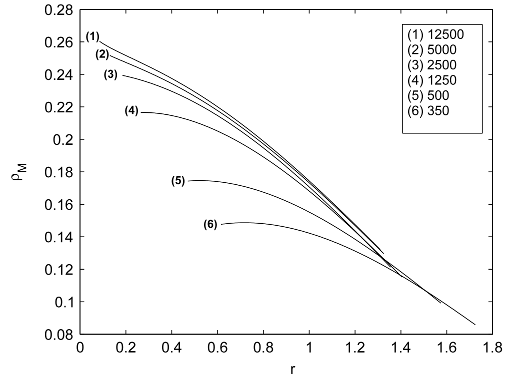

(a) Mill solutions for varying $\frac{\beta\lambda}{\alpha}$.

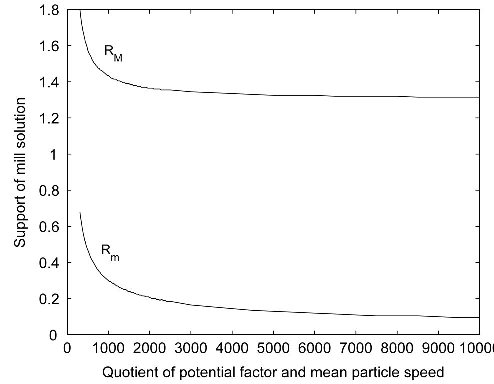

(b) Support of mill solutions for varying $\frac{\beta\lambda}{\alpha}$.

Fig. 7. Quasi-Morse potentials with identical shape parameters C, l, k result in mill solutions with different support sizes and densities, depending on the ratio of potential factor and squared stationary speed of the mill.

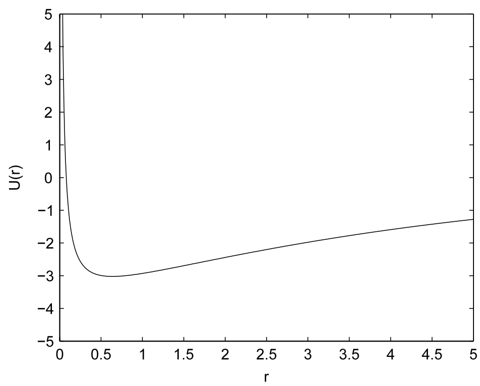

(a) Quasi-Morse potential in 3D.

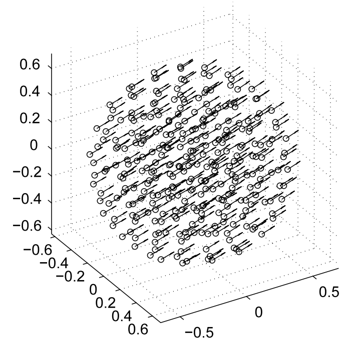

(b) 3D flock emerged in a particle simulation with $N = 200$ particles.

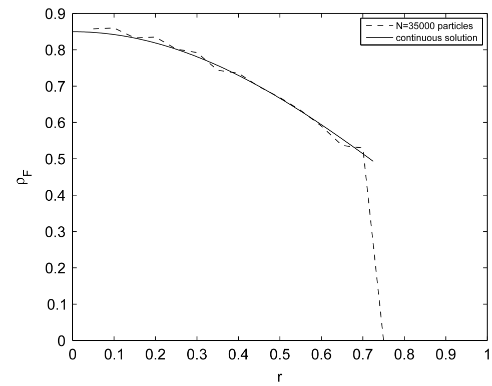

(c) 3D radial flock density: continuous result vs. empirical measure ($N = 35\,000$ particles).

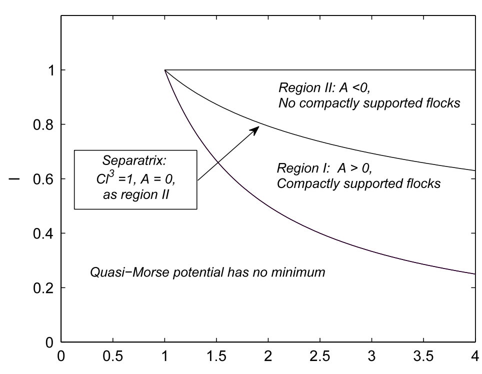

(d) Parameter diagram.

Fig. 8. The Quasi-Morse potential in three dimension is able to produce aligned flock solutions. The continuous radial density can be expressed as $\rho_F = \mu_1 \cdot \sin(ar)\frac{1}{r} + \mu_2 \cdot 1$ with, in this case, $\mu_1 \approx 0.3574$, $\mu_2 \approx 0.0052$, $R_F \approx 0.725$, $A = 5.585$. Our result is verified by comparing to the empirical density obtained from a particle simulation. (a) Exemplary potential shape, (b) flock emerged from 3D particle simulation, (c) continuous flock solution vs empirical measure, (d) parameter diagram of biological relevant configurations.

arrangements or "finite particle" flocks as in Section 4.2. Next we study the impact of parameters α, β, λ on the stationary mill solution, which enter the solution solely in the joint quotient $\frac{\alpha}{\lambda\beta}$. Hence, for a potential multiplied by a factor λ, the mill solution will stay the same, if the preferred speed of particles is multiplied by $\sqrt{\lambda}$ by any suitable change of α and/or β. In Fig. 7(a), we show several mill densities for our standard potential configuration and $\frac{\beta}{\lambda\alpha} \in \{350, 500, 1250, 2500, 5000, 12\,500\}$. The support of mill solutions is plotted against $\frac{\beta}{\lambda\alpha}$ in Fig. 7(b).

4.4. Flocks in 3D

The introduction of Quasi-Morse potentials enables us also to study flocks in three space dimensions. As we have mentioned in Section 3, the area of admissible parameter configurations is smaller than in the 2D case, as illustrated in the parameter diagram. For our example, we set $C = 1.255$, $l = 0.8$, $k = 0.2$, $A = 5.585$ and plot the resulting potential shape in Fig. 8(a). A three-dimensional flock resulting from a particle simulation is shown in Fig. 8(b). With the help of Algorithm 1 the continuous radial flock density is computed as a linear combination of $\frac{\sin ar}{r}$ and a constant. Notice that, due to Remark 3, Algorithm 3 is not needed. Also in three dimensions, the empirical density of a particle simulation matches our result, as illustrated in Fig. 8(c). Concerning the existence of flock solutions in the dependence of the shape parameters C and l, we get an equivalent picture as in two dimensions (see Fig. 8(d)): Though different in shape, the area of biologically relevant shapes is divided into two subregions by the separatrix $Cl^3 = 1$. In region I, continuous compactly supported three-dimensional flocks are found, not so in region II, which again indicates H-stability. Here, flocks do appear but their support increases with the total number of agents N. In the special case of the separatrix, which can be investigated with the computation of the case $A = 0$ in Section 3, no flock solutions are found.

5. Discussion

Quasi-Morse potentials fulfill three properties desirable from biological modeling: short-term repulsion, long-term attraction and vanishing interaction at infinity. Using Quasi-Morse potentials instead of the standard Morse potential makes, in our view, hardly any difference in terms of biological modeling. The stronger singularity at the origin for $n \neq 2$ might even be desirable in order to enforce repulsion. Though the special functions involved for $n = 2$ may seem not as convenient to work with as the exponential function, the existence of continuous, compactly supported stationary states itself make Quasi-Morse potentials a good choice for further studies of the models discussed in the above. Our results are, to the best of our knowledge, one of the first of its kind for explicit solutions of flock and mill patterns in two or three dimensions. The strategy of building up potentials from solutions of certain partial differential equations might work in other cases as well, and form one tool in the effort to understand the equilibria of interaction potentials. However, the techniques applied here are of no help for general potentials, such as classical Morse. With a variety of potentials suggested (see the discussion in Section 2), the problem of choosing the best suited one for a particular biological application becomes increasingly evident and should be a topic of future research.

6. Conclusions

In this paper, we have introduced the Quasi-Morse interaction potentials for a second-order model of self-propelled interactive particles. The Quasi-Morse potentials lead to the emergence of flocks and mills, similar to the standard Morse potential. We have shown that the radial densities of these stationary states are (affine) linear combinations of two or three elementary functions, which are chosen with respect to the three subcases $A > 0$ (catastrophic), $A = 0$ (separatrix) or $A < 0$. In order to determine the correct scalar coefficients and the a priori unknown support, we have developed a numerical algorithm that does not use time evolutions in Section 4. We have illustrated our result with examples for flocks and mills in two dimension and flocks in 3D. In all cases, our findings are convincingly verified by corresponding particle simulations. With our algorithm, we find that for all coherent patterns, only the catastrophic scenarios $A > 0$ lead to continuous compactly supported solutions.

Acknowledgments

JAC acknowledges partial support by MICINN project, reference MICINN MTM2011-27739-C04-02, by GRC 2009 SGR 345 by the Generalitat de Catalunya, and by the Engineering and Physical Sciences Research Council grant number EP/K008404/1. JAC also acknowledges support from the Royal Society through a Wolfson Research Merit Award. We also acknowledge the Isaac Newton Institute for the Mathematical Sciences, where part of this work was accomplished. We are grateful to Yanghong Huang for several useful comments.

Appendix

This appendix is devoted to the proof of Corollary 2. Denote by $V_k(r)$ the potential in (12) for a given $k > 0$. Notice that, $V_k(r) = k^{n-2}V_1(kr)$, hence we set $k = 1$ without loss of generality and, from now on, we drop the index k for simplicity.

Let us first show, the assertion about the unique minimum of the potential. This property is desirable from the biological point of view to set a typical length scale for the distance between agents.

Let $U(r) = V(r) - CV\left(\frac{r}{l}\right)$, then $U'(r) = V'(r) - \frac{C}{l}V'\left(\frac{r}{l}\right)$, and the necessary condition for a local extremum can be stated as finding r such that

$$h(r) := \frac{C}{l}\frac{V'\left(\frac{r}{l}\right)}{V'(r)} = 1.$$

Straightforward computations lead to

$$\begin{aligned} h'(r) &= \frac{C}{l(V'(r))^2}\left(\frac{1}{l}V''\left(\frac{r}{l}\right)V'(r) - V'\left(\frac{r}{l}\right)V''(r)\right) \\ &= \frac{C}{l(V'(r))^2}\left(-\frac{n-1}{r}V'(r)V'\left(\frac{r}{l}\right) + \frac{1}{l}V\left(\frac{r}{l}\right)V'(r) + \frac{n-1}{r}V'(r)V'\left(\frac{r}{l}\right) - V(r)V'\left(\frac{r}{l}\right)\right) \\ &= \frac{C}{l(V'(r))^2}\left(\frac{1}{l}V'(r)V\left(\frac{r}{l}\right) - V'\left(\frac{r}{l}\right)V(r)\right), \end{aligned}$$

where we used that V is a solution of $\frac{n-1}{r}V'(r) + V''(r) = V(r)$.

We next check that, $\log(-V(r))$ is a convex function of r for $n = 1, 2, 3$. Indeed, if $n = 1$, then $\log(-V(r))$ is affine; if $n = 3$, then $\log(-V(r)) = -\log r - r - \log(4\pi)$. In the case $n = 2$, we have

$$(\log(-V(r)))'' = \frac{K_0(x)^2 + K_2(x)K_0(x) - 2K_1(x)^2}{2K_0(x)^2},$$

and we can use the inequality $K_0(x)^2 + K_2(x)K_0(x) - 2K_1(x)^2 > 0$ (which can be verified numerically).

Thus, if $l < 1$, we have $\frac{V'(\frac{r}{l})}{V(\frac{r}{l})} \geq \frac{V'(r)}{V(r)}$. Since $V(r) < 0$, $V'(r) > 0$, this implies $V'(\frac{r}{l})V(r) - V'(r)V(\frac{r}{l}) \geq 0$, and therefore

$$\begin{aligned} h'(r) &= \frac{C}{l(V'(r))^2}\left(\frac{1}{l}V'(r)V\left(\frac{r}{l}\right) - V'\left(\frac{r}{l}\right)V(r)\right) \\ &< \frac{C}{l(V'(r))^2}\left(V'(r)V\left(\frac{r}{l}\right) - V'\left(\frac{r}{l}\right)V(r)\right) \leq 0. \end{aligned}$$

Similarly, if $l > 1$, we obtain $h'(r) > 0$.

Further, it is directly checked that

$$\lim_{r\to 0+} h(r) = Cl^{n-2} \quad \text{and} \quad \lim_{r\to\infty} h(r) = \begin{cases} 0 & \text{if } l < 1 \\ +\infty & \text{if } l > 1. \end{cases}$$

Thus, the equation $h(r) = 1$ has no solution in the cases $Cl^{n-2} < 1,\ l < 1$ or $Cl^{n-2} > 1, l > 1$ and a unique positive solution in the cases $Cl^{n-2} < 1,\ l > 1$ or $Cl^{n-2} > 1, l < 1$. Recalling that $U'(r) = V'(r)(1 - h(r))$, we see that of the last two cases, the former corresponds to a local maximum of $U(r)$ and the latter to a local minimum. Since the minimum is unique, then it is a global minimum.

Concerning the second assertion, by construction we have

$$\int_{\mathbb{R}^n} V(|x|)\mathrm{d}x = -1 \quad \text{for all } n,$$

since V is the fundamental solution of $\Delta u - u = \delta_0$ as stated in Definition 3. Therefore, we get

$$\int_{\mathbb{R}^n} U(|x|)\mathrm{d}x = \int_{\mathbb{R}^n} V(|x|) - CV(|x|/l)\mathrm{d}x = -1 + Cl^n,$$

which is negative for $Cl^n < 1$, and thus U is catastrophic (see [27, p. 37]).

References

[1] J. Parrish, L. Edelstein-Keshet, Complexity, pattern, and evolutionary trade-offs in animal aggregation, Science 294 (1999) 99–101.
[2] A. Mogilner, L. Edelstein-Keshet, L. Bent, A. Spiros, Mutual interactions, potentials, and individual distance in a social aggregation, J. Math. Biol. 47 (2003) 353–389.
[3] E. Bonabeau, M. Dorigo, G. Theraulaz, Swarm Intelligence: From Natural to Artificial Systems, Oxford University Press, New York, 1999, Intelligence: From Natural to Artificial Systems.
[4] S. Camazine, J.-L. Deneubourg, N.R. Franks, J. Sneyd, G. Theraulaz, E. Bonabeau, Self-Organization in Biological Systems, Princeton University Press, 2003.
[5] I.D. Couzin, J. Krause, N.R. Franks, S.A. Levin, Effective leadership and decision making in animal groups on the move, Nature 433 (2005) 513–516.
[6] I.D. Couzin, J. Krause, R. James, G. Ruxton, N. Franks, Collective memory and spatial sorting in animal groups, J. Theoret. Biol. 218 (2002) 1–11.
[7] A. Huth, C. Wissel, The simulation of the movement of fish schools, J. Theoret. Biol. 152 (1992) 365–385.
[8] H. Kunz, C.K. Hemelrijk, Artificial fish schools: collective effects of school size, body size, and body form, Artif. Life 3 (2003) 237–253.
[9] C.K. Hemelrijk, H. Kunz, Density distribution and size sorting in fish schools: an individual-based model, Behav. Ecol. 16 (2005) 178–187.
[10] A. Barbaro, K. Taylor, P.F. Trethewey, L. Youseff, B. Birnir, Discrete and continuous models of the dynamics of pelagic fish: application to the capelin, Math. Comput. Simul. 79 (2009) 3397–3414.
[11] A. Barbaro, B. Einarsson, B. Birnir, S. Sigurthsson, H. Valdimarsson, O.K. Palsson, S. Sveinbjornsson, T. Sigurthsson, Modelling and simulations of the migration of pelagic fish, ICES J. Mar. Sci. 66 (2009) 826–838.
[12] H. Hildenbrandt, C. Carere, C.K. Hemelrijk, Self-organised complex aerial displays of thousands of starlings: a model, Behav. Ecol. 21 (6) (2010) 1349–1359.
[13] Y.X. Li, R. Lukeman, L. Edelstein-Keshet, Minimal mechanisms for school formation in self-propelled particles, Physica D 237 (2008) 699–720.
[14] Y.X. Li, R. Lukeman, L. Edelstein-Keshet, A conceptual model for milling formations in biological aggregates, Bull. Math. Biol. 71 (2008) 352–382.
[15] M. Ballerini, N. Cabibbo, R. Candelier, A. Cavagna, E. Cisbani, L. Giardina, L. Lecomte, A. Orlandi, G. Parisi, A. Procaccini, M. Viale, V. Zdravkovic, Interaction ruling animal collective behavior depends on topological rather than metric distance: evidence from a field study, Proc. Natl. Acad. Sci. USA 105 (2008) 1232–1237.
[16] Y. Katz, K. Tunstroem, C. Ioannou, C. Huepe, I.D. Couzin, Inferring the structure and dynamics of interactions in schooling fish, Proc. Natl. Acad. Sci. USA 108 (2011) 18720–18725.
[17] T. Vicsek, A. Czirok, E. Ben-Jacob, I. Cohen, O. Shochet, Novel type of phase transition in a system of self-driven particles, Phys. Rev. Lett. 75 (1995) 1226–1229.
[18] G. Grégoire, H. Chaté, Onset of collective and cohesive motion, Phys. Rev. Lett. 92 (2004) 025702.
[19] P. Degond, S. Motsch, Continuum limit of self-driven particles with orientation interaction, Math. Models Methods Appl. Sci. 18 (2008) 1193–1215.
[20] H. Levine, W.J. Rappel, I. Cohen, Self-organization in systems of self-propelled particles, Phys. Rev. E 63 (2000) 017101.
[21] M.R. D'Orsogna, Y.L. Chuang, A.L. Bertozzi, L. Chayes, Self-propelled particles with soft-core interactions: patterns, stability, and collapse, Phys. Rev. Lett. 96 (2006) 104302.
[22] J.A. Carrillo, M. Fornasier, G. Toscani, F. Vecil, Particle, kinetic, and hydrodynamic models of swarming, in: Mathematical Modeling of Collective Behavior in Socio-Economic and Life Sciences, in: Series: Modelling and Simulation in Science and Technology, Birkhäuser, 2010, pp. 297–336.
[23] J.A. Cañizo, J.A. Carrillo, J. Rosado, Collective behavior of animals: swarming and complex patterns, Arbor 186 (2010) 1035–1049.
[24] A. Bernoff, C. Topaz, A primer of swarm equilibria, SIAM J. Appl. Dyn. Syst. 10 (1) (2011) 212–250.
[25] Y.L. Chuang, M.R. D'Orsogna, D. Marthaler, A.L. Bertozzi, L. Chayes, State transitions and the continuum limit for a 2D interacting, self-propelled particle system, Physica D 232 (2007) 33–47.
[26] Y.L. Chuang, Y.R. Huang, M.R. D'Orsogna, A.L. Bertozzi, Multi-vehicle flocking: scalability of cooperative control algorithms using pairwise potentials, in: IEEE International Conference on Robotics and Automation, 2007, pp. 2292–2299.
[27] D. Ruelle, Statistical Mechanics: Rigorous Results, W. A. Benjamin, Inc., New York-Amsterdam, 1969.
[28] J.A. Carrillo, A. Klar, S. Martin, S. Tiwari, Self-propelled interacting particle systems with roosting force, Math. Models Methods Appl. Sci. 20 (2010) 1533–1552.
[29] J.A. Carrillo, M.R. D'Orsogna, V. Panferov, Double milling in self-propelled swarms from kinetic theory, Kinet. Relat. Models 2 (2009) 363–378.
[30] R. Dobrushin, Vlasov equations, Funct. Anal. Appl. 13 (1979) 115–123.
[31] H. Neunzert, The Vlasov equation as a limit of Hamiltonian classical mechanical systems of interacting particles, Trans. Fluid Dynam. 18 (1977) 663–678.

[32] W. Braun, K. Hepp, The vlasov dynamics and its fluctuations in the 1/N limit of interacting classical particles, Comm. Math. Phys. 56 (1977) 101–113.
[33] H. Spohn, Large Scale Dynamics of Interacting Particles, in: Texts and Monographs in Physics, Springer, 1991.
[34] J.A. Cañizo, J.A. Carrillo, J. Rosado, A well-posedness theory in measures for some kinetic models of collective motion, Math. Models Methods Appl. Sci. 21 (2011) 515–539.
[35] F. Bolley, J.A. Cañizo, J.A. Carrillo, Stochastic mean-field limit: non-Lipschitz forces & swarming, Math. Models Methods Appl. Sci. 21 (2011) 2179–2210.
[36] M. Hauray, P.-E. Jabin, Particles approximations of Vlasov equations with singular forces: part 2, Preprint.
[37] D. Balagué, J.A. Carrillo, T. Laurent, G. Raoul, Nonlocal interactions by repulsive-attractive potentials: radial ins/stability, Physica D 260 (2013) 5–25.
[38] K. Fellner, G. Raoul, Stable stationary states of non-local interaction equations, Math. Models Methods Appl. Sci. 20 (2010) 2267–2291.
[39] K. Fellner, G. Raoul, Stability of stationary states of non-local interaction equations, Math. Comput. Modelling 53 (2011) 1436–1450.
[40] R.C. Fetecau, Y. Huang, T. Kolokolnikov, Swarm dynamics and equilibria for a nonlocal aggregation model, Nonlinearity 24 (2011) 2681–2716.
[41] E. Hackett-Jones, K. Landman, K. Fellner, Aggregation patterns from non-local interactions: discrete stochatic and continuum modelling, Phys. Rev. E 85 (2012) 041912.